Ecological Indicators 60 (2016) 483–494

Contents lists available at ScienceDirect

Ecological Indicators

journal homepage: www.elsevier.com/locate/ecolind

Detection of sensitive soil properties related to non-point phosphorus pollution by integrated models of SEDD and PLOAD

Chen Lin[a,b,*], Zhipeng Wu[c], Ronghua Ma[a], Zhihu Su[a,d]

[a] Key Laboratory of Watershed Geographic Sciences, Institute of Geography and Limnology, Chinese Academy of Sciences, Nanjing 210008, China
[b] State Key Laboratory of Soil and Sustainable Agriculture, Institute of Soil Science, Chinese Academy of Sciences, Nanjing 210008, China
[c] School of Geographic and Oceanographic Sciences, Nanjing University, Nanjing 210046, China
[d] College of Geography and Environmental Sciences, Zhejiang Normal University, Jinhua, Zhejiang Province 321004, China

ARTICLE INFO

Article history:
Received 2 March 2015
Received in revised form 7 July 2015
Accepted 26 July 2015

Keywords:
Non-point source pollution
Phosphorus loads
Soil erosion
Critical soil properties
Taihu Lake

ABSTRACT

Effectively identifying soil properties in relation to non-point source (NPS) phosphorus pollution is important for NPS pollution management. Previous studies have focused on particulate P loads in relation to agricultural non-point source pollution. In areas undergoing rapid urbanization, dissolved P loads may be important with respect to conditions of surface infiltration and rainfall runoff. The present study developed an integrated model for the analysis of both dissolved P and particulate P loads, applied to the Meiliang Bay watershed, Taihu Lake, China. The results showed that NPS P loads up to 15 kg/km^2 were present, with particulate P loads up to 13 kg/km^2. The highest loads were concentrated in the southeastern region of the watershed. Although particle P was the main contributor to NPS P loads state, the contribution of dissolved P was significant, especially in sub-basins with significant amount of artificial land cover. The integration of dissolved P and particulate P loads provided more accurate evaluation of NPS P pollution. NPS P loads were found to correspond to specific soil properties. Soil organic matter and total nitrogen were shown to influence dissolved P loads, while total phosphorus and soil particle composition proportion were more closely related to particulate P loads.

© 2015 Elsevier Ltd. All rights reserved.

1. Introduction

Phosphorus (P) is an essential element for crop growth and a primary nutrient of inland lakes (Norton et al., 2012). Excessive discharge of P can significantly affect water quality (Smith et al., 2001; Delpla et al., 2011). In recent decades, the non-point source (NPS) P loading has become a priority for water pollution management in many catchments (Evanylo et al., 2008; Yang, 2009a,b), in relation to lake eutrophication. In order to control water eutrophication, reducing P discharge is considered an effective solution (Castoldi et al., 2009). Therefore, understanding NPS P pollution loads and control factors are important for the protection of the watershed environment.

Identifying spatial P pollution loads is an important aspect of managing catchment related eutrophication. A large number of NPS models have been developed (Table 1). In general, these can be divided into two categories: empirical models (SWAT, ANSWERS, and AGNPS, etc.) and the physically based models (RUSLE, SEDD, and PLOAD, etc.) (Laurent and Ruelland, 2011; Beasley et al., 1980; Wang et al., 2012; Shen et al., 2011; Gburek and Sharpley, 1998). The physically based models have shown accurate estimation of pollutants in small spatial scale, but are limited due to complexity and excessive reliance on detailed field observations. These make these models less unsuitable for large spatial scales (McDowell et al., 2002; Bechmann et al., 2009). Empirical models are widely used in watershed monitoring with various advantages such as condensed structures, accessible parameters and simple and efficient operation (He et al., 2011, 2012).

The NPS P loads are categorized as: particulate loads under agriculture non-point source pollution (ANPS) condition and the dissolved loads under impervious surface runoff, in which the soil P is lost from the particulate state (sediment adsorption state). Many studies determine particulate P loads by classical empirical models, in particular the Universal Soil Loss Equation (RUSLE), which has been widely applied to evaluate soil erosion modulus by integrating several factors including climate, land use, soil, topography, vegetation and enrichment ratio of sediment pollutants

* Corresponding author at: Key Laboratory of Watershed Geographic Sciences, Institute of Geography and Limnology, Chinese Academy of Sciences, Nanjing 210008, China. Tel.: +86 25 86882169; fax: +86 25 83592686.
E-mail addresses: clin@niglas.ac.cn (C. Lin), rhma@niglas.ac.cn (R. Ma).

http://dx.doi.org/10.1016/j.ecolind.2015.07.023
1470-160X/© 2015 Elsevier Ltd. All rights reserved.

Table 1
Commonly used NPS models.

Models	Type	Output information	Required parameters
SWAT	Physically based	The pollutants (total nitrogen and total phosphorus) delivery process, including three modules such as runoff, soil erosion and river delivery.	Rainfall, runoff, evaporation, channel attenuation, silt and sediment deposit, cultivation measures, land use, soil texture, soil composition, soil organic matter, soil total nitrogen, soil total phosphorus, etc.
AGNPS	Physically based	Nutrient material circulation driven by agriculture non-point source pollution, the output information was grid and pixel based.	Rainfall, runoff, soil infiltration rate, sediment deposit, land use, fertilizer consumption, total phosphorus and total nitrogen contents in fertilizers and pesticides, soil moisture, etc.
RUSLE	Classical empirical	The soil loss amounts	Land use, soil type, rainfall, slope, vegetation status
SEDD	Classical empirical	The amounts of nutrients loss in particulate state	Soil loss amounts, sediment delivery ratio, nutrients concentration status in sediment
PLOAD	Classical empirical	The loss amounts of nutrients in runoff	Rainfall, land use, pollutants concentration in runoff

(Terranova et al., 2009; Ouyang et al., 2010). Based on the fundamental form of RUSLE, the sediment delivery distributed (SEDD) model has been recently improved by researchers (Fu et al., 2006; Jain and Kothyari, 2000). One of the improvements is to take sediment delivery factor into account, and thereby the loss of soil sediment absorbed nutrients can be quantitatively and more precisely monitored (Yang et al., 2012). More importantly, under rapid urbanization in eastern China in recent decades, the increased impermeable land surfaces in these areas impact overall surface infiltration and rainfall runoff, and cause soil nutrients to be lost in the dissolved state (Ouyang et al., 2012). Therefore, dissolved P loss has gained more attention in large scale NPS research (Wang et al., 2014). The PLOAD model is a generic GIS-based NPS screening model proposed by USEPA (2003) and has been widely used in simulation of runoff coefficients under storm conditions, suggesting that the PLOAD could be an ideal choice for dissolved P loss assessment of dissolved pollutant concentrations (Lee et al., 2008; Kemanian et al., 2011). Above all, as dissolved P (Dis-P) and particulate P loads (Par-P) constitute the entire NPS P loads (Tot-P), an effective model should integrate them for the accurate assessment of NPS P loads, especially in urban-rural mixed regions (Cui et al., 2003). In this context the SEDD and PLOAD approaches represent an ideal choice.

Based on the assessment and monitoring results of NPS P loads, studies have demonstrated that NPS P pollution load is influenced by rainfall, topography, land use, soil properties, hydrologic process and human activities (Strauss et al., 2007; Razafindrabe et al., 2010; Petrosell et al., 2014; Wu et al., 2012). Soil erodibility factor (K) has been used to represent the impact of land use and rainfall features on soil characteristics, and also demonstrate the critical influence on NPS P loads status directly (Recanatesi et al., 2013). The erodibility factor can be calculated by identifying soil organic matter content and soil mechanical composition. Therefore, the soil properties including soil organic matter (SOM), soil acidity, soil nutrients and soil particle composition influence NPS P loads, and more information on the relationship between NPS P and critical soil properties is needed.

With the rapid urbanization and significant land use change, the watershed of Meiliang Bay has experienced the most severe eutrophication. This watershed is a typical urban–rural mixed area in Yangtze River Delta and Taihu basin and suffers from severe NPS pollution (Duan et al., 2015). The objectives of the present study are: (i) assess the watershed P loss status based on the model that considers both dissolved P and particulate P loads together; (ii) analyze relationships of Dis-P and Par-P to the total P loads (Tot-P) and the underlying soil properties. The results from this study provide fundamental information for managing NPS in mixed use watersheds.

2. Materials and methods

2.1. Study site

The watershed region of Meiliang Bay is located in the eastern coast of China and south of the Yangtze River Delta, the area is 486.2 km^2. This region is located in a peri-urban area between Wuxi and Changzhou cities, which have undergone massive economic development and changing agricultural land use. The study area has undergone rapid urbanization in the last 30 years, and a large number of arable lands and forestlands were replaced by artificial land cover (Li et al., 2007). Nowadays, more than 30% of the area is impervious surface and 55% is arable land. The average annual precipitation at the study area is 1035 mm, and the main rainfall season is from May to October. The annual mean runoff depth is 688 mm and the annual average temperature is 15.6 °C. The main soil type in this area is bleached paddy soil, which covers more than 85% of the study site. Soil organic matter (SOM), total P (TP), total nitrogen (TN) content is 1.97 g kg^{-1}, 0.07 g kg^{-1} and 0.12 g kg^{-1} respectively. Sand proportion accounts for 13.14% and pH is 5.97 (Gong et al., 2003). Moreover, the sub-watershed has a dense river network, consisting of three trunk streams with their tributaries such as Wujin Port, Yangxi and Liangxi Rivers, which flow into Meiliang Bay of the Taihu Lake. Eighteen sub-basins were generated by ArcGIS based on three inflow rivers (Fig. 1).

2.2. Quantitative evaluation of NPS P loads

2.2.1. Adsorbed NPS P loads component

The SEDD model was used to assess the NPS particulate P loads, which was followed with the basic Revised Universal Soil Loss Equation (RUSLE), attached sediment factor and sediment delivery ratio into the model formulation (Cui et al., 2003; Yang et al., 2012). The model was calculated in ArcGIS using 30 m × 30 m spatial grids

$$Par\ (P) = A_i \times P_{sed} \times SDR_i \quad (1)$$

where $Par(P)$ is the particulate P load per unit area (kg km^{-2} $year^{-1}$); P_{sed} expresses the sediment total P concentration status (g kg^{-1}); SDR_i is the sediment delivery ratio (%) for each grid, which is calculated based on the following model:

$$SDR_i = \exp(-\beta t_i) \quad (2)$$

where t_i is the travel time (h) from the grid i to the nearest river channel along the flow path and β is a coefficient lumping together the effects of roughness and runoff along the flow path (Ferro, 1997). The sensitivity of SDR to β is watershed-specific, and the value of 0.304 was used because this value produces smallest mean relative square error between modeled and measured sediment yield (Guo et al., 2004; Strauss et al., 2007; Zhou and Wu, 2008). Travel time was calculated (Eq. (3)) (Jain and Kothyari, 2000), using

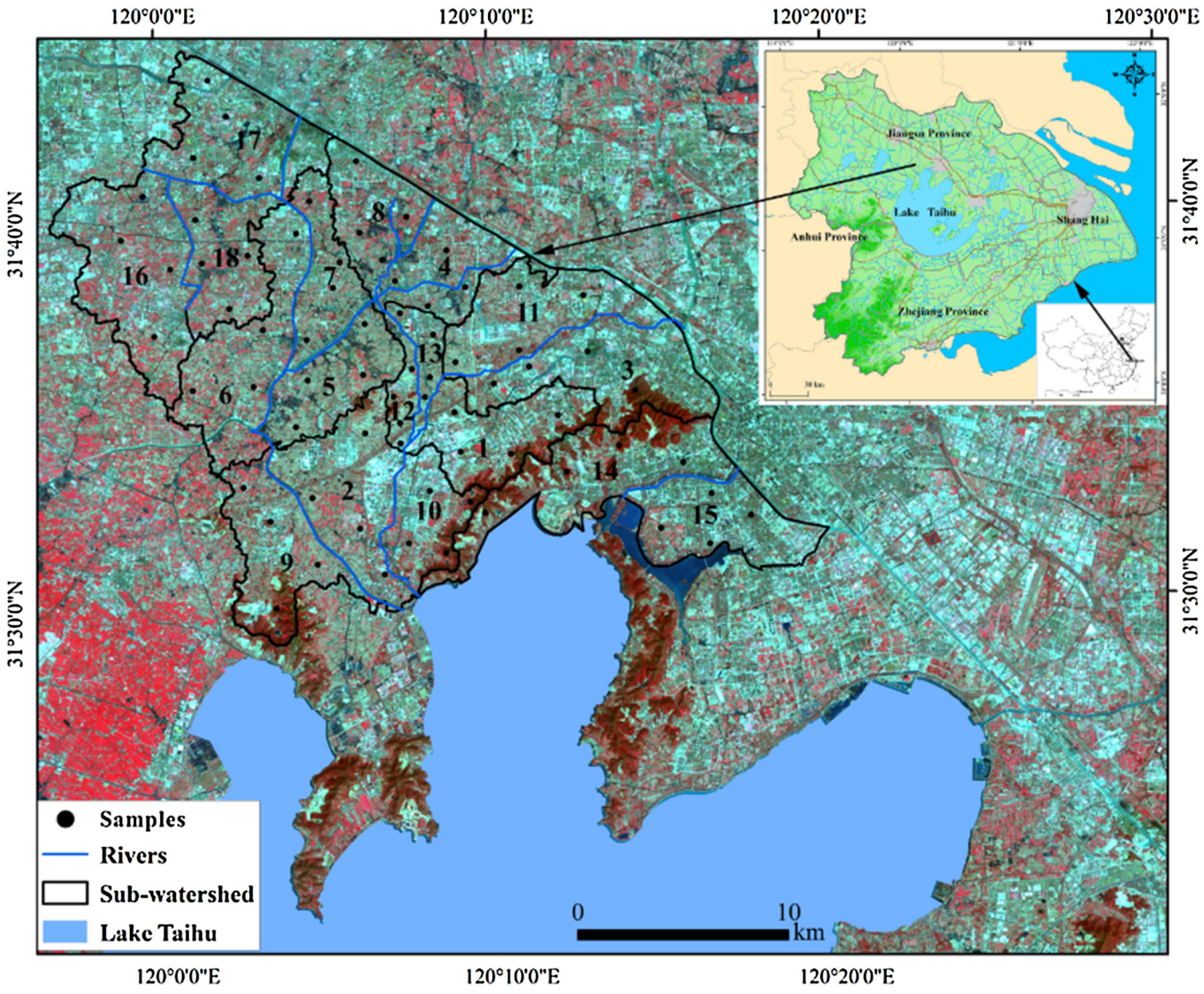

Fig. 1. Location of study site and sampling plots.

l_j as the flow length and v_j as a velocity factor derived from Smith and Maidment (1995)

$$t_i = \sum_{j=1}^{N_P} \left(\frac{l_j}{v_j} \right) \tag{3}$$

The soil erosion modulus (Ai, kg km^{-2} year^{-1}) was calculated by RUSLE.

$$A_i = R_i \times K_i \times LS_i \times C_i \times P_i \tag{4}$$

where R_i is the rainfall-runoff erosivity factor (MJ mm (ha h year)$^{-1}$); K_i is the soil erodibility factor (Mg h MJ^{-1} mm^{-1}); LS_i is the slope length and steepness factor; C_i is the cover management factor; and P_i is the conservation support practice factor based on land use (Dabarl et al., 2008). The algorithm of the R factor used in this study is given by (Wischmeier and Smith, 1987) the following:

$$R = \sum_{n=1}^{12} 1.735 \times 10^{(1.5 \times lg(P_i^2/P) - 0.8188)} \tag{5}$$

where P_i is the monthly average rainfall (mm) and P is the annual average rainfall (mm). The K value was assigned by the soil type spatial distribution map (1:1,000,000) made by Bu et al. (2002) in Taihu Basin.

The factor LS reflects the effects of topography on soil erosion, and is the acceleration factor of erosion power. LS factors include slope length and steepness factors. The L and S were extracted from ASTER global DEM data, the spatial accuracy was 30 m and calculated according to McCool et al. (1987) and Onyando et al. (2005), where θ is the slope angle in degrees, and λ is the field slope length (m).

$$L = (\lambda/22.13)^m = \begin{cases} m = 0.2 & \theta < 0.5^\circ \\ m = 0.3 & 0.5^\circ \le \theta < 1.5^\circ \\ m = 0.4 & 1.5^\circ \le \theta < 3^\circ \\ m = 0.5 & \theta \ge 3^\circ \end{cases}$$

$$S = \begin{cases} 10.8 \sin(\theta) + 0.03 & \theta \le 5^\circ \\ 16.8 \sin(\theta) + 0.5 & 5^\circ < \theta < 10^\circ \\ 21.9 \sin(\theta) + 0.03 & \theta \ge 10^\circ \end{cases} \tag{6}$$

P is determined as the ratio between the soil losses expected for certain soil conservation practice, based on land use type. In

Table 2
Goodness-of-fit statistical data for model's validation.

	Annual mean yield		R^2	E_{NS}
	Observed	Simulated		
Tot-P (t year^{-1})	31.254	28.109	0.940	0.892
Sediment (10^4 t year^{-1})	1.694	1.524	0.966	0.911
Par-P (t year^{-1})	17.424	14.037	0.967	0.850
Dis-P (t year^{-1})	15.746	14.073	0.961	0.856

Table 3
The data source for NPS P loads calculation.

Data type	Data source	Description
Land use	Second National Land Survey of China	The land use types in the study area were interpreted in the second national land survey of China, the data source were the Resource Satellite ST.3 (ZY-3) images, and the data production prepared in the end of 2012. The data were merged into six main types for the convenience of the study (forestland, arable land, orchard land, wetland, construction land and other land) (Fig. 3). Moreover, several modeling factors including conservation support practice factor (P), runoff coefficient (Rn), P_{dis} and C_{sed} were assigned based on the six land use types.
Satellite images	Landsat Enhanced Thematic Mapper (ETM+) data	The data was acquired from USGS, and the satellites transit date is August 2, 2013, the closest date to actual sampling period. The spatial accuracy was 30 m. The NDVI data was interpreted from the image, which was the basis of the cover-management factor (C) assignment.
Soil type	<Soil Annals of Jiangsu Province>	The data were digitized from the publication of <Soil Annals of Jiangsu Province>, and the soil erodibility factor (K) was assigned based on the soil type.
Digital elevation model (DEM)	ASTER global DEM	The data were acquired from USGS, and the spatial accuracy was 30 m. The length-slope factor (LS) was calculated from the length and slope spatial data.
Runoff amount	Meteorological monitoring stations in Taihu Basin	Four monitoring stations were located in study sites, and the runoff data of 2013 were collected daily. The average annual rainfall amount was acquired and then interpolated into spatial scale. The rainfall intensity (R) factor was calculated from the spatial rainfall data.

this study, the P was taken on Xu et al. (2012), for Taihu's basin. C is defined as the cover-management factor, which expresses the protective effect of soil cover against the erosive action of rainfall. The C factor was calculated (Durigon et al., 2014) using a regression equation derived from correlation analysis between the factor C measured in the field and a satellite-derived NDVI.

2.2.2. Dissolved NPS P loads

The PLOAD model is a GIS-based model used to calculate non-point source pollutant loads from different sub-watersheds and lands based on annual or seasonal precipitation and land uses (CH2M-HILL). The algorithms consist of the Simple Method and Export Coefficient models (USEPA, 2003). In the present study, the PLOAD model was used to estimate dissolved non-point source nutrient load using:

$$Dis(P) = P_i \times P_{j_i} \times Rn_i \times C_{run} \quad (7)$$

where $Dis(P)$ is the dissolved non-point source nutrient loads per unit area (kg km^{-2} year^{-1}) for each pixel i; P_i is precipitation (mm year^{-1}); Pj_i is ratio of storm producing runoff (default = 0.9) (Cui et al., 2003; Shi et al., 2012); Rn_i is runoff coefficient for land use type; C_{run} is event mean concentration (EMC) for different land use types (mg L^{-1}). The runoff coefficient (Rn) was evaluated based on each land use type within different sub-basins, and derived with the following equation:

$$Rn = 0.05 + (0.009 \times I_{imp}) \quad (8)$$

where I_{imp} is imperious factor for different land uses and the value is selected from the guidelines provided by NRCCS, TR-55 user's manual (USEPA, 2001). C_{run} is represented by EMC, which occurs in the runoff from specific event by taking the flow sample at regular interval during the event from runoff using following equation:

$$EMC = \frac{\sum P_{dis} Q_n}{\sum Q_i} \quad (9)$$

where P_{dis} is the concentration of sample n and Q_n is flow rate. Flow rate (Q_n) of each example is obtained after the generation of surface runoff from each event of rainfall using PLOAD simulation. P_{dis} was assigned based on different sub-basins and land use types. The runoff samples were obtained after typical rainfall events, corresponding to certain land use pattern for different sub-basins. Surface runoff samples were filtered through a 0.7-μm precombusted glass fiber filters (25-mm diameter; Whatman GF/F), and the filtrate was used to determine dissolved phosphorus. The dissolved phosphorus concentrations were measured in soil and environment analysis center, Institute of Soil Science, Chinese Academy of Sciences, and analyzed with inductively coupled plasma-atomic emission spectrometry (ICP-AES) (Lin et al., 2008).

2.2.3. NPS P loads assessment and validation

Total NPS-P loads were determined by adding dissolved and adsorbed components, as follows:

$$Tot(P) = \left(\sum_i^n Par(P) + \sum_i^n Dis(P) \right) \times A_U \quad (10)$$

where $Tot(P)$ is the introduction of NPS nutrients into the rivers (kg year^{-1}) and A_U is area of land use type (km^2) within each sub-basin. The model was implemented in ArcGIS 10.0 based on raster grid (30 × 30), and then clustered into each sub-basin.

To validate the model, the in situ measurements from monitoring sites in the outlet of each sub-watershed were used to compare actual and modeled sediment and runoff discharge of the sub-watershed under severe rainfall conditions (average values

Table 4
Values of factors P_{sed} and P_{dis} for different land use types.

Land use type	P_{sed} (g kg^{-1})	P_{dis} (mg kg^{-1})
Forestland	0.323	0.241
Arable land	0.424	0.192
Orchard land	0.518	0.072
Construction land	0.012	0.354
Wetland	0.233	0.172
Grass land	0.318	0.135
Others	0.342	0.239

from four measurements per year). The Nash–Sutcliffe coefficient (*Ens*) was used to assess the performance of the model (Nash and Sutcliffe, 1970):

$$E_{NS} = 1 - \frac{\sum_{i=1}^{N}(Q_{obs,i} - Q_{sim,i})^2}{\sum_{i=1}^{N}(Q_{obs,i} - \bar{Q}_{obs})^2} \quad (11)$$

where $Q_{obs,i}$ and $Q_{sim,i}$ are the observed and predicted values, respectively. Q_{obs} is the mean observed values within eighteen sub-basins, and the $Q_{sim,I}$ is the mean simulated values within eighteen sub-basins.

The observed and simulated values for Par-P, Dis-P, Tot-P and sediment loss amount were distributed uniformly along the 1:1 line (Fig. 2). R^2 for Par-P, Dis-P and sediment discharge were elevated, with R^2 for Tot-P slightly lower than the other three indices (Table 2). The *Ens* score were reached 0.9. The validation indicated that the model simulated accurately the phosphorus and sediment for the watershed for the entire year, and a close agreement between the observed and simulated phosphorus and sediment discharge amounts were also revealed during the model validation.

2.3. Data collection

The spatial data of modeling factors and soil properties were used in the modeling calculation for NPS P loads (Table 3).

It is worth to mention that indices of P_{sed} and P_{dis} were assigned based on land use data. Specifically, the two factors were acquired by sample measurements in different land use types of each sub-basin (Table 4).

The soil properties, acquired from field sampling and laboratory measurements, were used to analyze the relationships between critical soil properties and NPS P loads. Surface soil samples (0–10 cm depth) were collected during October 22–24, 2013, just after the freezing period and before the plowing season. In eighteen sub-basins, four sampling sites were selected; these sites covered three critical land use patterns including forestland, arable land and orchard land. The sampling sites were 150–200 m apart (using a global positioning system) to ensure spatial uniformity (Fig. 1). In each site, soils were sampled 9 times within a radius of 20 m apart from the plot center, and were then mixed into a single sample. Soil samples were air dried and grinded prior to analysis for soil total phosphorus (TP), total nitrogen (TN), pH, soil organic matter (SOM) and soil particle composition were measured. Specially, the pH was measured by potentiometric method. The TP and TN concentrations were measure with inductively coupled plasma-atomic emission spectrometry (ICP-AES) (Lin et al., 2008). The SOM was determined after oxidation by potassium bichromate and sulphuric acid solution and measured by an external heating method (Houba et al., 1989). The contents of sand (0.05–2 mm), silt (0.002–0.05 mm) and clay (0–0.002 mm) particles in soil were measured following the pipette method (Soil Science Society of China, 2000). Finally, the measurements of four samples in the same sub-basin were averaged to represent the soil properties of the target sub-basin.

2.4. Relationship between soil properties and NPS P loads in sub-basin scale

To analyze the relationships between NPS P loads and soil properties, Pearson correlation analysis was performed using SPSS 19.0, and the correlation coefficients (r) were used to evaluate the existing relationships. To identify the critical soil indicators that were sensitive to Par-P, Dis-P and Tot-P loads, a stepwise regression analysis was conducted between different NPS P loads (dependent variable) and soil properties (independent variable) at 0.05 and 0.01 levels. T test was used to identify the significance of the independent variables coefficients ($p \leq 0.05$) that entered in the final stepwise model (Basnyat et al., 1999; Ferguson et al., 2008).

3. Results

3.1. Spatial features of NPS P loads

According to SEDD and PLOADS models realized in GIS environment, the spatial distribution of NPS P loads is mapped in Fig. 4.

The results (Fig. 4) show that dissolved P ranged from 0.0083 to 3.531 kg/km^2, particulate P ranged from 0 to 12.747 kg/km^2, and Tot-P loads amounts ranged from 0 to 15.332 kg/km^2.

Par-P loads (Table 5) ranged from 5.686 to 31.968 t year^{-1}, the dis-P loads ranged from 3.368 to 23.640 t year^{-1}, and the total P loads ranged from 9.053 to 49.584 t year^{-1}. The intensity of Par-P ranged from 0.227 to 1.210 t/km^2/year, whereas the intensity of Dis-P varied little from 0.391 to 0.794 t/km^2/year among different sub-basins.

Among different sub-basins, No. 11 and No. 13 sub-basins were under severe Par-P pollution load with average intensities greater than 1.0 t/km^2/year. Sub-basins No. 15 and No. 3 were under the most severe Dis-P pollution with average intensities greater than 0.64 t/km^2/year. Importantly, the total P pollution distribution shared the same tendency of Par-P, with extreme pollution areas concentrated in the south-eastern region, including No. 11 and No. 13 sub-basins. However, when both Par-P and Dis-P loads were considered, sub-basins No. 2, 5, 12 and 15 also suffered from serious NPS P pollution.

3.2. Spatial pattern of soil properties

To be consistent with the NPS data, the spatial data of soil properties were clustered according to sub-basin boundaries (Table 6).

SOM content, TP and TN were 2.00 g kg^{-1} (1.07–2.66 g kg^{-1}), 0.160 g kg^{-1} (0.097–0.195 g kg^{-1}), and 0.159 g kg^{-1} (0.066–0.255 g kg^{-1}), respectively. In general, the tendency TP content in different sub-basins was similar to the tendency of TN, and TP was greater than the regional background level. In addition, SOM content varied significantly among different sub-basins, and the average content was basically equal to the background value. The average pH was 6.0, which was slightly higher than the average background level. With respect to soil particle composition, silt proportions in the soil samples were much higher than the proportions of sand and clay with an order of silt > sand > clay. Sand proportion increased compared with the background status (Gong et al., 2003).

The contents of SOM, TN and TP showed a similar spatial distribution with high values in No. 6, 7 and 8 sub-basins in central north of the area and mostly covered with arable land. The content of SOM was high in No. 9, 10 and 14 sub-basins in southern area with forest land use. Unlike other properties, soil pH and soil particle composition showed little variation among different sub-basins.

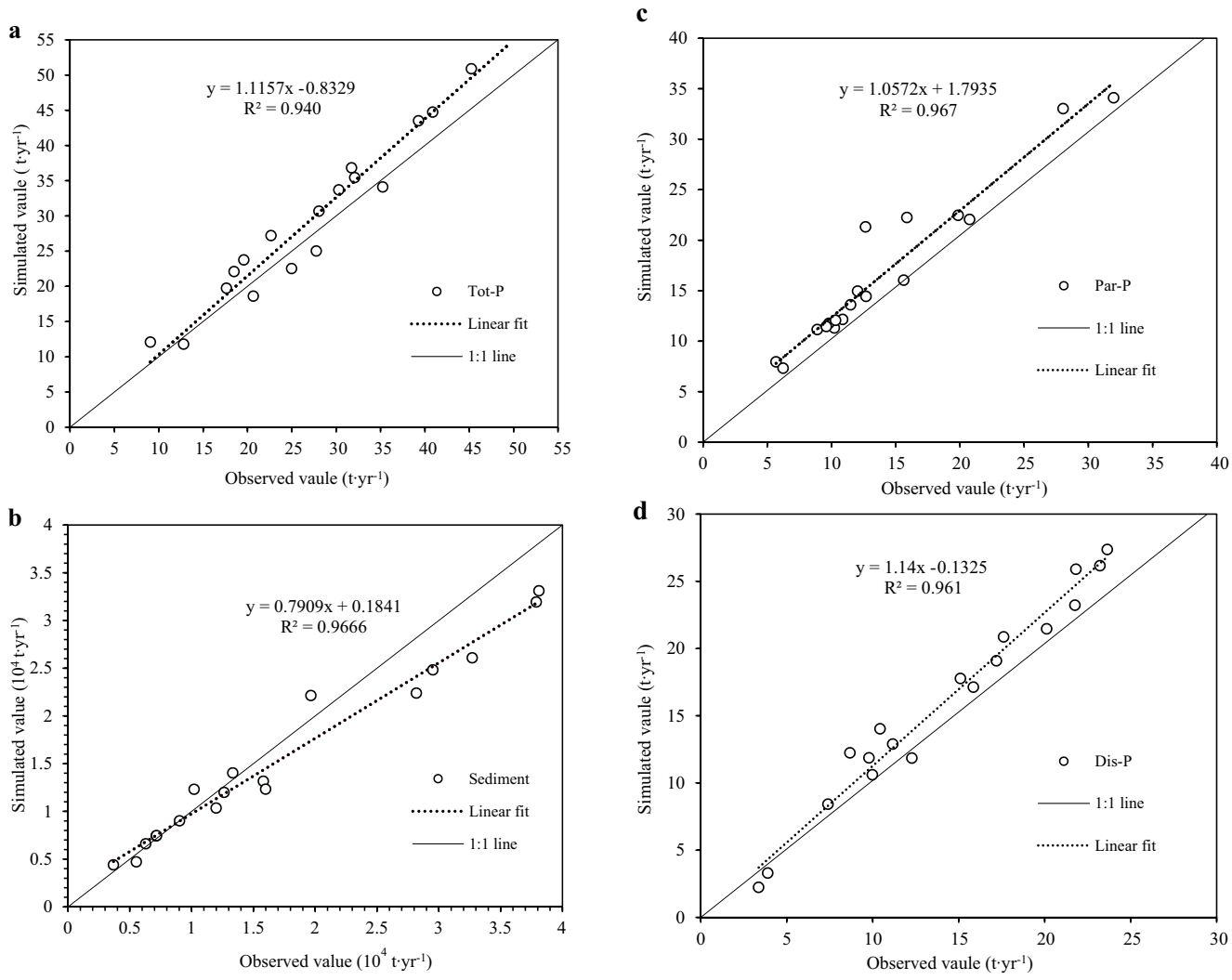

Fig. 2. Scatter diagram of observed and predicted values within eighteen sub-basins.

Table 5
The statistical data of NPS P loads within different sub-basins.

Sub-basin	Area (km^2)	Par-P		Dis-P		P loads	
		Loads (t $year^{-1}$)	Average intensity (t/km^2/year)	Loads	Average intensity (t/km^2/year)	Loads	Average intensity (t/km^2/year)
1	27.27	12.656	0.463	15.101	0.554	27.757	1.018
2	35.17	28.042	0.797	17.197	0.489	45.239	1.286
3	36.47	15.633	0.429	23.640	0.648	39.273	1.077
4	22.28	11.485	0.516	11.167	0.501	22.653	1.017
5	22.62	19.863	0.877	10.428	0.461	30.291	1.339
6	37.76	15.877	0.420	15.852	0.420	31.730	0.840
7	18.94	10.229	0.540	7.400	0.391	17.628	0.931
8	21.08	10.872	0.516	9.787	0.464	20.659	0.980
9	29.31	12.690	0.433	12.279	0.419	24.970	0.852
10	19.06	9.807	0.514	8.679	0.455	18.486	0.970
11	30.22	31.968	1.059	17.617	0.583	49.584	1.641
12	6.21	5.686	0.916	3.368	0.542	9.053	1.458
13	7.34	8.897	1.210	3.897	0.531	12.794	1.742
14	39.52	10.321	0.261	21.762	0.551	32.084	0.812
15	27.48	6.241	0.227	21.818	0.794	28.059	1.021
16	44.48	12.035	0.271	23.217	0.522	35.252	0.793
17	35.36	20.759	0.588	20.121	0.569	40.880	1.156
18	24.76	9.599	0.387	9.979	0.403	19.579	0.791

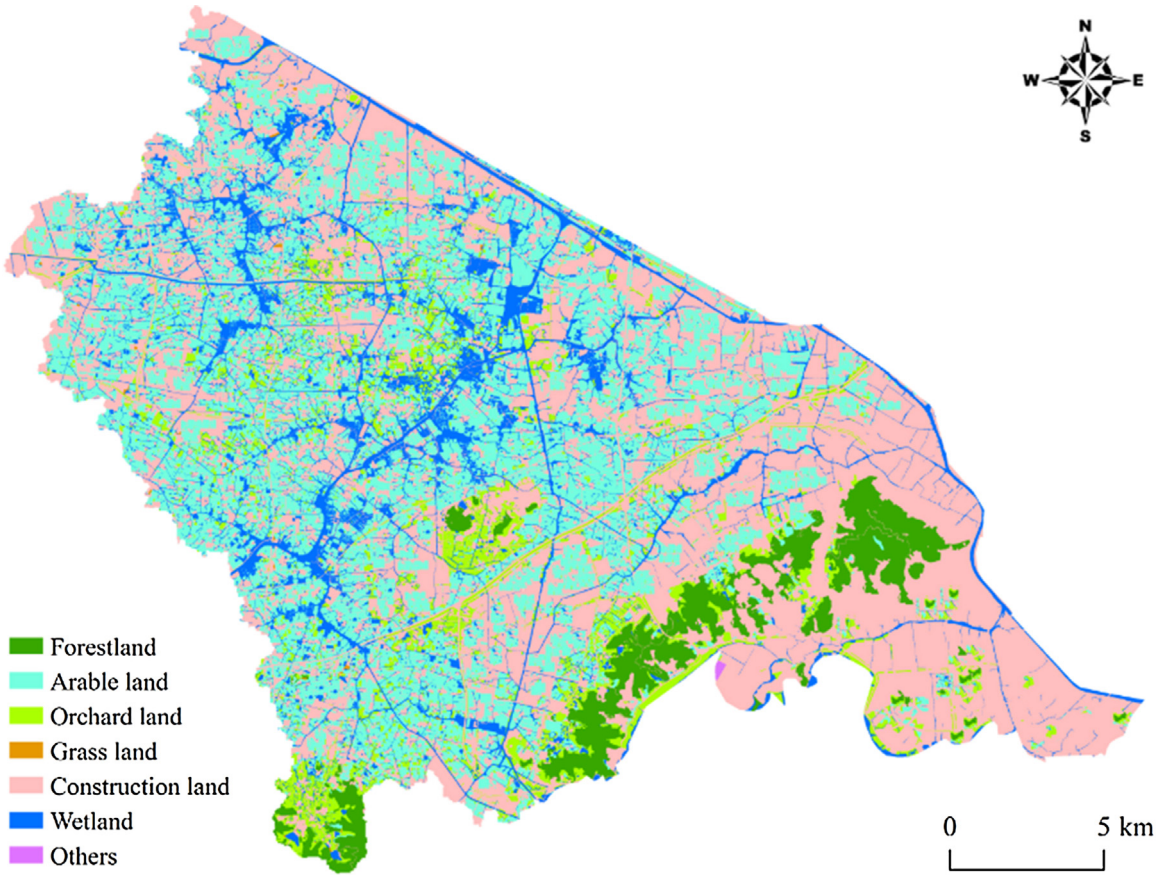

Fig. 3. The map of land use patterns (data from second national land survey of China 2012).

Table 6
Soil properties within different sub-basins.

Sub-basin	TP (g kg^{-1})	SOM (g kg^{-1})	TN (g kg^{-1})	pH	Sand (%) (0.05–2 mm)	Silt (%) (0.002–0.05 mm)	Clay (%) (<0.002 mm)
1	0.185	2.266	0.162	6.470	15.668	76.280	8.069
2	0.155	1.966	0.180	6.080	17.555	75.383	6.973
3	0.190	1.447	0.066	6.640	18.163	76.375	6.391
4	0.194	2.303	0.155	6.370	16.513	75.475	8.019
5	0.146	2.144	0.157	5.794	17.288	78.060	4.706
6	0.182	2.563	0.179	6.020	15.218	77.640	7.143
7	0.205	2.533	0.255	6.010	14.788	79.075	6.705
8	0.184	2.648	0.196	5.630	15.455	80.250	5.516
9	0.157	2.109	0.182	5.930	14.788	78.260	6.919
10	0.172	2.580	0.127	6.030	14.721	76.500	8.873
11	0.106	2.037	0.153	6.000	19.259	75.033	6.07
12	0.138	1.238	0.179	5.890	18.188	75.100	6.791
13	0.097	1.756	0.164	6.300	18.388	77.667	4.09
14	0.151	2.664	0.115	6.220	14.013	78.007	8.057
15	0.156	1.065	0.102	6.000	13.988	80.900	5.489
16	0.158	2.569	0.161	5.990	15.14	78.100	7.032
17	0.105	1.255	0.189	5.880	17.788	76.025	6.141
18	0.193	2.146	0.146	5.830	12.738	79.467	7.805
Average	0.160	2.072	0.159	6.016	16.092	77.422	6.71

Table 7
Correlation coefficients (r) between NPS P loads and soil properties.

	TP (g kg^{-1})	SOM (g kg^{-1})	TN (g kg^{-1})	pH	Sand (%) (0.05–2 mm)	Silt (%) (0.002–0.05 mm)	Clay (%) (<0.002 mm)
par-P	−0.63**	−0.25	0.26	0.05	0.79**	−0.47*	−0.53
dis-P	−0.32	−0.66**	−0.63**	0.21	0.24	−0.02	−0.27
Tot-P	−0.72**	−0.47*	0.03	0.19	0.84**	−0.47	−0.61**

* $p < 0.05$.
** $p < 0.01$.

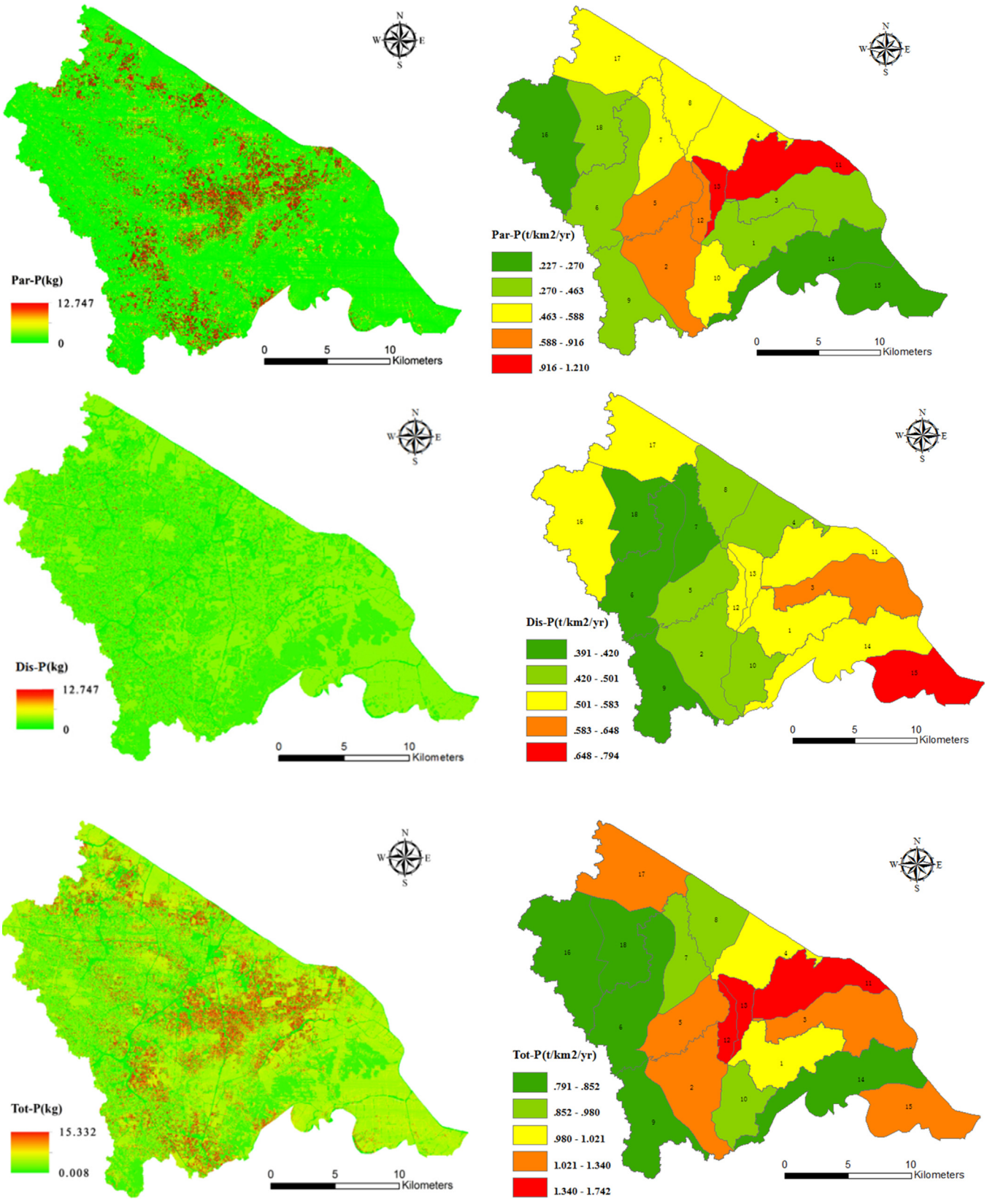

Fig. 4. The spatial distribution of NPS P loads (a: the particulate P loads; b: the particulate P loads in each sub-basin; c: the dissolved P loads; d: the dissolved P loads in each sub-basin; e: P loads integrated with particulate P and dissolved P; f: P loads in each sub-basin).

3.3. Relationship between NPS P loads and soil properties

Results showed that SOM, TP and sand proportion were significantly related to P loads (Table 7). The correlation coefficient for TP and sand proportion was as high as 0.8. However, the differences of the correlation between soil properties and loads from different P types were notable. Firstly, the status of Par-P was similar to the total P loads. TP and sand proportion had the greatest correlation coefficients (−0.78 and 0.75) with Par-P, while SOM and TN were closely related to Dis-P loads with correlation coefficients of −0.73 and −0.69, respectively.

Multiple stepwise regressions were performed between selected soil properties and various NPS P loads to better understand the sensitivity of soil properties to NPS P loads (Table 8).

The Tot-P modeling results were similar to the Par-P results, both of them introduced two independent variables such as TP and sand contents into the regression models. The R^2 value of Tot-P was better than that of Par-P. For Dis-P loads, TN and SOM were used, allowing for a lower R^2 than the Tot-P and Par-P models.

4. Discussion

4.1. Contribution of Par-P and Dis-P to NPS P loads

Studies show that NPS P loads are closely related to soil P nutrients, especially TP concentration, which is more strongly correlated to NPS P loads than Olsen-P (Chung et al., 2003). In this study, the correlation coefficient between TP content and Par-P loads was −0.63 within eighteen sub-basins (Table 7). However, the correlation coefficient increased to 0.72 when Dis-P loads were taken into consideration with Par-P; the relation between TP content and Dis-P loads was less strong than that of Par-P. The results show that the integration of SEDD and PLOAD provides a more accurate assessment, possibly because Dis-P loads are linked to NPS P loads, especially in urban-rural regions.

The results also indicted that the particulate P was still the main source of NPS P loads. Fig. 4 indicates that the maximum value of Par-P loads is 1.210 t/km^2/year, while the maximum value of Dis-P loads is 0.8 t/km^2/year. The spatial distribution of Tot-P loads was largely determined by Par-P loads, in which the severely pollution region was located in northern and center of the study area, and the medium pollution regions were concentrated in western area.

The proportions for Par-P and Dis-P loads to the total NPS P loads varied markedly within different sub-basins (Fig. 5). Par-P loads proportions in twelve sub-basins exceeded 50% and accounted for up to 69% in No. 13 sub-basin. Previous studies showed that arable land, forestland and orchard land produced more NPS P loads than the other land use patterns due to excessive fertilizer usage and soil erosion (Ahearn et al., 2005). Given this, the proportions of arable land and orchard land with different sub-basins were consistent with the Par-P load model results. For instance, in the No. 5, 11 and 13 sub-basins with the highest Par-P loads, arable land and orchard land occupied more than 55% of the basin areas, far more than artificial land cover (construction land, Fig. 3). However, the contribution of Dis-P loads was more significant than Par-P in several sub-basins, particularly in No. 14 and No. 15. These two sub-basins in the southeast were largely covered by impervious surface, which were more prone to dissolved phosphorus runoff. Furthermore, the Dis-P also influenced the spatial distribution of the Tot-P loads in some sub-basins (e.g., No. 15 and No. 17), where the NPS P loads pollution intensity was evidently increased while they were not severely polluted when the Par-P loads were considered solely (Fig. 4). Past studies suggested that nearly 80% portion of P loss was in particulate form within the whole Taihu Lake watershed (Yang, 2009a,b). Our results suggest that the importance of Par-P load may decrease as the impervious area increases.

In conclusion, the NPS P pollution was generated by combination of particulate P and dissolved P loads, in which the particulate P still accounted for the larger proportion with relation to land use. The effect of dissolve P loads was most important in areas of elevated impervious surface related to urbanization.

4.2. The critical soil properties related to NPS P loads

Many factors including land use/cover change (LUCC), soil background and present status, agriculture irrigation and P fertilization can impact on NPS P loads. Among them, soil properties are a main factor for NPS P pollution as soil physical and chemical properties directly affect soil P loading and watershed nutrients flux (Kim et al., 2009). Therefore, it is useful to identify which soil property is the most sensitive and how different this property can affect the NPS loads for different P types.

Soil TP is widely used as direct indicative targets for NPS P loading. Soil TP is typically negatively correlated with NPS P loading (Ouyang et al., 2012). This was confirmed in the present study. TP was the main factor to interpret Par-P and Tot-P loads along with the sand proportion (Tables 7 and 8).

Soil organic matter is designated as the most critical soil property affecting nutrient concentration dynamics (Grabs et al., 2009). In this study, the content of SOM in soil was unsurprisingly much higher than the other nutrients. SOM was negative correlated with Dis-P loads ($r = -0.66$), and showed no significant level with respect to Par-P. SOM was not introduced as the main component to interpret Tot-P. These findings indicated that the importance of SOM was less than that reported in related studies (Navas et al., 2012). From the scatter plots between SOM contents and corresponding Par-P and Dis-P loads within eighteen sub-basins (Fig. 6), the relation between SOM and P loads did not follow a linear tendency. Par-P and SOM contents were poorly fitted when SOM was lower than 2.4 g kg^{-1}, while a negative relationship became clear when the SOM reached 2.53 g kg^{-1}. The tendency was reversed with respect to Dis-P, confirming studies showing that SOM and NPS P loads are closely linked when soil SOM is higher than content 2.5 g kg^{-1} (Ben-Dor et al., 1997). This study also demonstrated that the opposite status is probably likely within Dis-P status, with the transition point of SOM content between 2.30 and 2.50 g kg^{-1}. Noticeably, only six sub-basins in the whole study area had SOM contents greater than 2.50 g kg^{-1}, and the relative low SOM contents in most of the sub-basins resulted in the relationship to be less ideal to Par-P loads than that to Dis-P loads.

Interestingly, the soil particle composition, especially the sand proportion, was closely related to Par-P loads ($r = 0.79$) and Tot-P loads ($r = 0.84$) (Table 7). The relationship between soil particle composition and non-point pollution has been rarely addressed (Braskerud, 2002; Vogel et al., 2010). We believe that two aspects could be inferred from our results. Firstly, the soil particle composition was closely related to Par-P load; higher proportion of sand, high Par-P loading. A reasonable explanation was that increased sand proportion as well as decreased clay proportion probably resulted from the loss and displacement of smaller soil particles from surface soil, causing land surface becoming rougher and prone to further soil erosion (Braskerud, 2003). In this case, the change of soil sand proportion is an indicator to NPS particulate P loads even though the sand was much lower in quantity than silt and clay. Secondly, in spite of the poor relationship between Dis-P and soil particle composition, the contribution of soil particle composition to the total P loads should not be neglected. The sand proportion was selected as one of the main variables to relate to Par-P and Tot-P as well as TP (Table 8). R^2 value increased to from 0.64 to 0.77 for Tot-P where both Par-P and Dis-P were considered together, rather

Table 8
The statistical data of the multiple stepwise regression results.

Loads from different P types	No. of introduced independents	Independents	R^2	RMSE
Par-P	2	TP, sand (%)	0.63	0.161
Dis-P	2	TN, SOM	0.61	0.605
Tot-P	2	TP, sand (%)	0.76	0.148

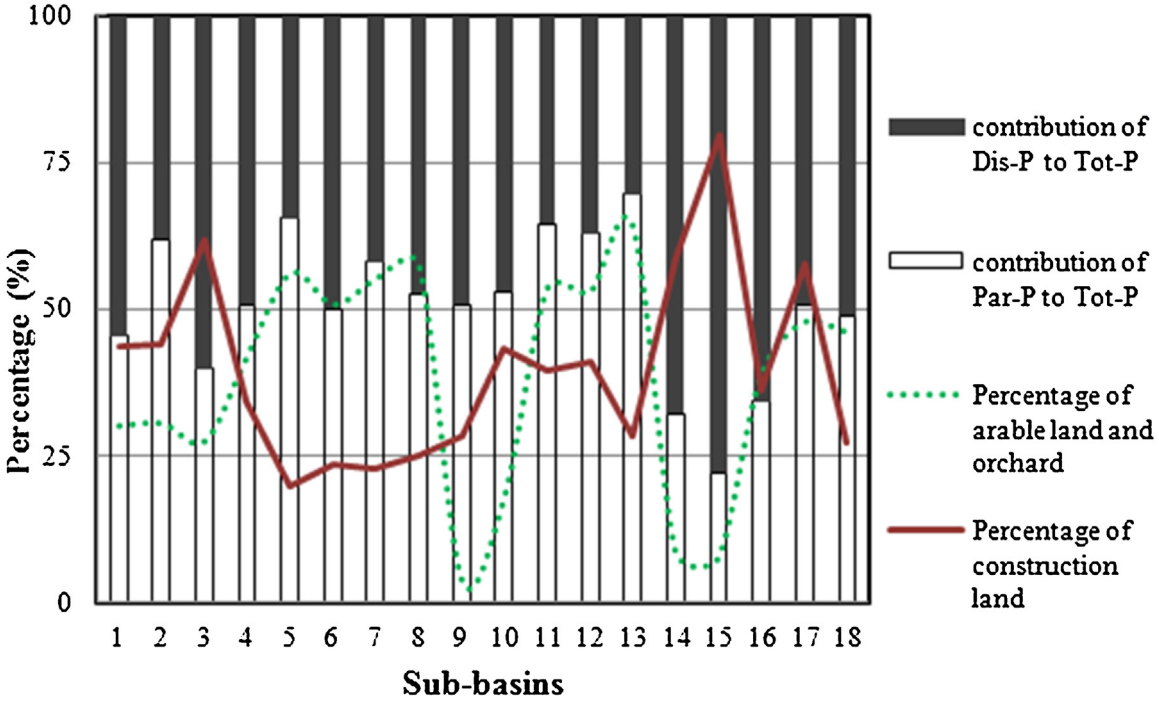

Fig. 5. The percentage of arable land and construction land and their relationship with NPS loads from different P types within each sub-basin.

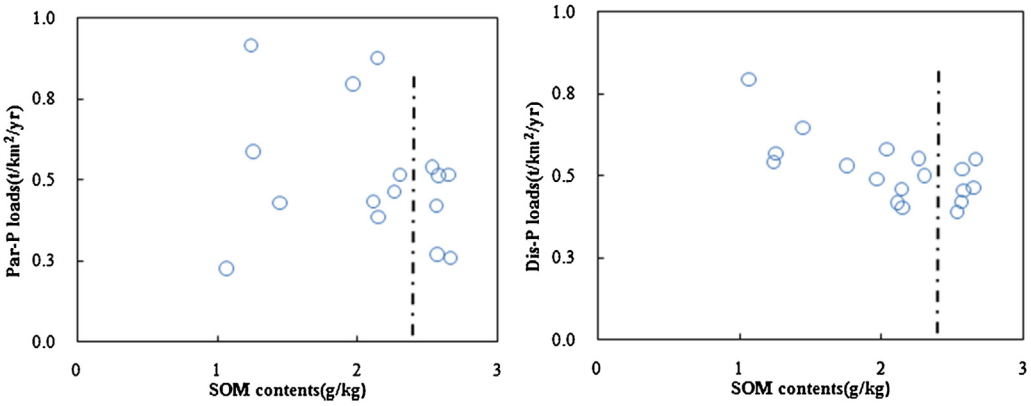

Fig. 6. The scatter points between SOM contents and NPS-P loads within different sub-basins.

than separately. These results suggested that the Dis-P loads probably had changed the general P load status in some sub-basins that possessed lighter Par-P loads, resulting in an overall better fitting effect.

4.3. Implication of NPS P load assessment

The NPS P pollution is designated as one of critical environmental problems in watersheds worldwide, and the NPS loading simulation is the first necessary step to understanding pollution management. The present study provided two important insights. Firstly, in NPS P loads assessment studies, particulate P loads should be considered as predominant factor, especially in agriculture regions. However, urbanization and climate change increase the importance of dissolved P loads in the total P load. Secondly, an understanding of the current status of soil properties and land use is necessary to determine P loads. Data acquisition by remote sensing allow for more accurate and recent information, in particular where land use change and urbanization rates are elevated. In economies under rapid development process, the corresponding NPS P loads vary on spatial and temporal scales. Rather than relying solely on historical data, updated information on soil properties and land use are necessary for effective watershed pollution management.

5. Conclusion

This study assessed the NPS P loading intensity by an integrated SEDD and PLOAD models, which considered both particulate and dissolved P loads. Results showed that the integration of these two types reflects general NPS P pollution more accurately due to better relationship with soil TP contents than the studies that considered the particulate P state pollution alone. More accurate and real-time soil property data and land use information was also essential for performance of NPS models. The study confirmed that particulate P remained was the main NPS P load, but pointed to the growing contribution of dissolved P loads in areas increasing impermeable land. The findings also suggested that the NPS P load in this important study area was more sensitive to soil nutrients and soil particle composition than the other factors. SOM and TN showed significant influence on Dis-P loads, whereas soil TP status and soil particle composition, especially the sand proportion, were more closely related to Par-P loads and Tot-P loads.

This study provides basic understanding of non-point source pollution in rural-urban mixed watershed. The findings implied that the management and optimization of cultivated areas, as well as improvement of fertilization technology, are necessarily for nutrient management in lake basins.

Acknowledgements

This work was funded by The National Natural Science Foundation of China (Grant No. 41301227) and Research Fund of State Key Laboratory of Soil and Sustainable Agriculture, Nanjing Institute of Soil Science, Chinese Academy of Science (Y412201427). Data were supported by Scientific Data Sharing Platform for Lake and Watershed, Nanjing Institute of Geography and Limnology, Chinese Academy of Sciences.

References

Ahearn, D.S., Sheibley, R.W., Dahlgren, R.A., Anderson, M., Johnson, J., Tate, K.W., 2005. Land use and land cover influence on water quality in the last free flowing river draining the western Sierra Nevada, California. J. Hydrol. 313 (3–4), 234–247.

Basnyat, P., Teeter, L.D., Lockaby, B.G., 1999. Relationships between landscape characteristics and nonpoint source pollution inputs to coastal estuaries. Environ. Manage. 23 (4), 539–549.

Ben-Dor, E., Inbar, Y., Chen, Y., 1997. The reflectance spectra of organic matter in the visible near-infrared and short wave infrared region (400–2500 nm) during a controlled decomposition process. Remote Sens. Environ. 61 (1), 1–15.

Bechmann, M., Stalnacke, P., Kvoerno, S., Eggestad, H.O., Oygarden, L., 2009. Integrated tool for risk assessment in agricultural management of soil erosion and losses of phosphorus and nitrogen. Sci. Total Environ. 407 (2), 749–759.

Beasley, D.B., Huggins, L.F., Monke, E.J., 1980. ANSWERS: a model for watershed planning. Trans. ASAE 23 (4), 938–944.

Braskerud, B.C., 2002. Factors affecting nitrogen retention in small constructed wetlands treating agricultural non-point source pollution. Ecol. Eng. 18 (3), 351–370.

Braskerud, B.C., 2003. Clay particle retention in small constructed wetlands. Water Res. 37 (16), 3793–3802.

Bu, Z.H., Yang, L.Z., Bu, Y.X., Wu, J.Y., 2002. Soil erodibility (K) value and its application in Taihu lake catchment. Acta Pedagog. Sin. 39 (3), 296–300 (in Chinese).

Castoldi, N., Bechini, L., Stein, A., 2009. Evaluation of the spatial uncertainty of agro-ecological assessments at the regional scale: the phosphorus indicator in northern Italy. Ecol. Indic. 9 (5), 902–912.

Chung, S.O., Kim, H.S., Kim, J.S., 2003. Model development for nutrient loading from paddy rice fields. Agric. Water Manage. 62 (1), 1–17.

Cui, G.B., Zha, H.E., Luo, J., 2003. Quantitative evaluation of non-point pollution of Taihu watershed using geographic information system. J. Lake Sci. 15 (3), 236–244 (in Chinese).

Dabarl, P.P., Baithuri, N., Pandey, A., 2008. Soil erosion assessment in a hilly catchment of North Eastern India using USLE, GIS and remote sensing. Water Resour. Manage. 22, 1783–1798.

Delpla, I., Baures, E., Jung, A.V., Thomas, O., 2011. Impacts of rainfall events on runoff water quality in an agricultural environment in temperate areas. Sci. Total Environ. 409 (9), 1683–1688.

Duan, H., Loiselle, S.A., Zhu, L., Feng, L., Zhang, Y., Ma, R., 2015. Distribution and incidence of algal blooms in Lake Taihu. Aquat. Sci. 1–8, http://dx.doi.org/10.1007/s00027-014-0367-2

Durigon, V.L., Carvalho, D.F., Antunes, M.A.H., Oliveira, P.T.S., Fernandes, M.M., 2014. NDVI time series for monitoring RUSLE cover management factor in a tropical watershed. Int. J. Remote Sens. 35 (2), 441–453.

Evanylo, G., Sherony, C., Spargo, J., Starner, D., Brosius, M., Haering, K., 2008. Soil and water environmental effects of fertilizer-, manure-, and compost-based fertility practices in an organic vegetable cropping system. Agric. Ecosyst. Environ. 127 (1–2), 50–58.

Ferguson, C.A., Carvalho, L., Scott, E.M., Bowman, A.W., Kirika, A., 2008. Assessing ecological responses to environmental change using statistical models. J. Appl. Ecol. 45, 193–203.

Ferro, 1997. Further remarks on a distributed approach to sediment delivery. Hydrol. Sci. J. 42, 633–647.

Fu, G.B., Chen, S.L., McCool, D.K., 2006. Modeling the impacts of no-till practice on soil erosion and sediment yield with RUSLE, SEDD, and ArcView GIS. Soil Till. Res. 85, 38–49.

Gburek, W.J., Sharpley, A.N., 1998. Hydrologic controls on phosphorus loss from upland agricultural watersheds. J. Environ. Qual. 27, 267–277.

Gong, Z.T., Chen, Z.C., Zhang, G.L., 2003. World reference base for soil resources (WRB): establishment and development. Soils 35 (4), 271–278 (in Chinese).

Grabs, T., Seibert, J., Bishop, K., Laudon, H., 2009. Modeling spatial patterns of saturated areas: a comparison of the topographic wetness index and a dynamic distributed model. J. Hydrol. 373 (1–2), 15–23.

Guo, H.Y., Wang, X.R., Zhu, J.G., 2004. Quantification and index of non-point source pollution in Taihu Lake region with GIS. Environ. Geochem. Health 26 (2), 147–156.

He, B., Kanae, S., Oki, T., Hirabayashi, Y., Yamashiki, Y., Takara, K., 2011. Assessment of global nitrogen pollution in rivers using an integrated biogeochemical modeling framework. Water Res. 45 (8), 2573–2586.

He, B., Oki, K., Wang, Y., Oki, T., Yamashiki, Y., Takara, K., Kawasaki, N., 2012. Analysis of stream water quality and estimation of nutrient load with the aid of Quick Bird remote sensing imagery. Hydrol. Sci. J. 57 (5), 850–860.

Houba, V.J.G., Van der, L.J.J., Novozamsky, I., Walinga, I., 1989. Soil and Plant Analysis, A Series of Syllabi: Part 5. Soil Analysis Procedures. Wageningen Agricultural University, The Netherlands.

Jain, M.K., Kothyari, U.C., 2000. Estimation of soil erosion and sediment yield using GIS. Hydrol. Sci. J. 45, 771–786.

Kemanian, A.R., Julich, S., Manoranjan, V.S., Arnold, J.R., 2011. Integrating soil carbon cycling with that of nitrogen and phosphorus in the watershed model SWAT: theory and model testing. Ecol. Model. 222 (12), 1913–1921.

Kim, H.J., Sudduth, K.A., Hummel, J.W., 2009. Soil macronutrient sensing for precision agriculture. J. Environ. Monit. 11 (10), 1810–1824.

Laurent, A., Ruelland, D., 2011. Assessing impacts of alternative land use and agricultural practices on nitrate pollution at the catchment scale. J. Hydrol. 409, 440–450.

Lee, K.S., Chung, E.S., Kim, Y.O., 2008. Integrated watershed management for mitigating streamflow depletion in an urbanized watershed in Korea. Phys. Chem. Earth 33, 382–394.

Li, Z.F., Yang, G.S., Li, H.P., 2007. Estimation of nutrient export coefficient from different land use types in Xitiaoxi watershed. Res. Soil Water Conserv. 21 (1), 1–4 (in Chinese).

Lin, C., He, M.C., Zhou, Y.X., Guo, W., Yang, Z.F., 2008. Distribution and contamination assessment of heavy metals in sediment of the Second Songhua River, China. Environ. Monit. Assess. 137, 329–342.

McCool, D.K., Foster, G.R., Mutchler, C.K., Meyer, L.D., 1987. Revised slope steepness factor for the universal soil loss equation. Trans. ASAE 30 (5), 1387–1396.

McDowell, R.W., Sharpley, A.N., Chalmers, A.T., 2002. Land use and flow regime effects on phosphorus chemical dynamics in the fluvial sediment of the Winooski River, Vermont. Ecol. Eng. 18, 477–487.

Nash, J., Sutcliffe, J.V., 1970. River flow forecasting through conceptual models. Part I – A discussion of principles. J. Hydrol. 10, 282–290.

Navas, A., Gaspar, L., Quijano, L., López-Vicente, M., Machín, J., 2012. Patterns of soil organic carbon and nitrogen in relation to soil movement under different land uses in mountain fields (South Central Pyrenees). Catena 94, 43–52.

Norton, L., Elliott, J.A., Maberly, S.C., 2012. Using models to bridge the gap between land use and algal blooms: an example from the Loweswater catchment, UK. Environ. Model. Softw. 36, 64–75.

Onyando, J.O., Kisoyan, P., Chemelil, M.C., 2005. Estimation of potential soil erosion for river Perkerra Catchment in Kenya. Water Resour. Manage. 19, 133–143.

Ouyang, W., Huang, H.B., Hao, F.H., Shan, Y.S., Guo, B.B., 2012. Evaluating spatial interaction of soil property with non-point source pollution at watershed scale: the phosphorus indicator in Northeast China. Sci. Total Environ. 432, 412–421.

Ouyang, W., Skidmore, A.K., Toxopeus, A.G., Hao, F.H., 2010. Long-term vegetation landscape pattern with non point source nutrient pollution in upper stream of Yellow River basin. J. Hydrol. 389 (3–4), 373–380.

Petrosell, A., Lenoe, A., Ripa, M.N., Recanatesi, F., 2014. Linking phosphorus export and hydrologic modeling: a case study in Central Italy. Environ. Monit. Assess. 186, 7849–7861.

Razafindrabe, B.H., He, B., Inoue, S., Ezaki, T., Shaw, R., 2010. The role of forest stand density in controlling soil erosion: implications to sediment-related disasters in Japan. Environ. Monit. Assess. 160 (1–4), 337–354.

Recanatesi, F., Ripa, M.N., Leone, A., Luigi, P., Luca, S., 2013. Land use, climate and transport of nutrients: evidence emerging from the Lake Vicocase study. Environ. Manage. 52, 503–513.

Shen, Z.Y., Hong, Q., Chu, Z., 2011. A framework for priority non-point source area identification and load estimation integrated with APPI and PLOAD model in Fujiang Watershed, China. Agric. Water Manage. 98, 977–989.
Shi, Q.L., Deng, X.Z., Wu, F., Zhan, J.Y., Xu, L.R., 2012. Best management practices for agricultural non-point source pollution control using PLOAD in Wuliangsuhai watershed. J. Food Agric. Environ. 10 (2), 1389–1393.
Smith, K.A., Jackson, D.R., Withers, P.J.A., 2001. Nutrient losses by surface run-off following the application of organic manures to arable land. Environ. Pollut. 112 (1), 53–60.
Smith, P.N.H., Maidment, D.R., 1995. Hydrologic data development system. CRWR Online Report No. 95-1. Center for Research in Water Resources, University of Texas, Austin, TX.
Soil Science Society of China, 2000. Methods of Soil Agrochemistry Analysis. Chinese Agriculture Science and Technology Press, Beijing (in Chinese).
Strauss, P., Leone, A., Ripa, M.M., Turpin, N., Lescot, J.M., Laplana, R., 2007. Using critical source areas for targeting cost-effective best management practices to mitigate phosphorus and sediment transfer at the watershed scale. Soil Use Manage. 23, 144–153.
Terranova, O., Antronico, R., Coscarelli, R., Iaquinta, P., 2009. Soil erosion risk scenarios in the Mediterranean environment using RUSLE and GIS: an application model for Calabria (southern Italy). Geomorphology 112, 228–245.
U.S.EPA, 2001. PLOAD User's Manual, Version 3. http://www.epa.gov/waterscience/BASINS/b3docs/PLOAD_v3.pdf (accessed 12.02.07).
U.S.-EPA, 2003. National Management Measures for the Control of Non-point Pollution from Agriculture. U.S.E.P. Agency, Washington, DC.
Vogel, H.J., Weller, U., Ippisch, O., 2010. Non-equilibrium in soil hydraulic modelling. J. Hydrol. 393 (1–2), 20–28.
Wang, H.J., Zhang, W.T., Song, H., Zhuang, Y.H., Lin, H.Y., Wang, Z., 2014. Spatial evaluation of complex non-point source pollution in urban–rural watershed using fuzzy system. J. Hydroinform. 16 (1), 114–129.
Wang, X.L., Wang, Q., Wu, C.Q., 2012. A method coupled with remote sensing data to evaluate non-point source pollution in the Xin'anjiang catchment of China. Sci. Total Environ. 430, 132–143.
Wischmeier, W.H., Smith, D.D., 1987. Predicting Rainfall Erosion Losses a Guide to Conservation Planning. USDA: US Department of Agriculture, Agricultural Handbook, Washington, DC, pp. 537.
Wu, L., Long, T.Y., Liu, X., Guo, J.S., 2012. Impacts of climate and land-use changes on the migration of non-point source nitrogen and phosphorus during rainfall-runoff in the Jialing River Watershed, China. J. Hydrol. 475, 26–41.
Xu, L.F., Xu, X.G., Meng, X.W., 2012. Risk assessment of soil erosion in different rainfall scenarios by RUSLE model coupled with information diffusion model: a case study of Bohai Rim, China. Catena 100, 74–82.
Yang, 2009a. Researches on Characteristics and Influencing Factors of Phosphorus Loss in Runoff in the Typical Land Use of Taihu Watershed. Zhejiang University press, Zhejiang, China (in Chinese).
Yang, L.X., 2009b. Researches on Characteristics and Influencing Factors of Phosphorous Loss in Runoff in the Typical Land Use of Taihu Watershed. Zhejiang University Press, pp. 45–54.
Yang, M., Li, X., Hu, Y.M., He, Y.Y., 2012. Assessing effects of landscape pattern on sediment yield using sediment delivery distributed model and a landscape indicator. Ecol. Indic. 22, 38–52.
Zhou, W.F., Wu, B.F., 2008. Assessment of soil erosion and sediment delivery ratio using remote sensing and GIS: a case study of upstream Chaobaihe River catchment, north China. Int. J. Sediment Res. 23 (2), 167–173.